

# Liquid drops attract or repel by the inverted Cheerios effect

Stefan Karpitschka<sup>a,1</sup>, Anupam Pandey<sup>a</sup>, Luuk A. Lubbers<sup>b</sup>, Joost H. Weijs<sup>c</sup>, Lorenzo Botto<sup>d</sup>, Siddhartha Das<sup>e</sup>, Bruno Andreotti<sup>f</sup>, and Jacco H. Snoeijer<sup>a,9</sup>

<sup>a</sup>Physics of Fluids Group, Faculty of Science and Technology, University of Twente, 7500 AE Enschede, The Netherlands; <sup>b</sup>Huygens-Kamerlingh Onnes Laboratory, Universiteit Leiden, Postbus 9504, 2300 RA Leiden, The Netherlands; <sup>c</sup>Université Lyon, Ens de Lyon, Université Claude Bernard, CNRS, Laboratoire de Physique, F-69342 Lyon, France; <sup>d</sup>School of Engineering and Materials Science, Queen Mary University of London, London E1 4NS, United Kingdom; <sup>e</sup>Department of Mechanical Engineering, University of Maryland, College Park, MD 20742; <sup>f</sup>Laboratoire de Physique et Mécanique des Milieux Hétérogènes, UMR 7636 École Supérieure de Physique et de Chimie Industrielles–CNRS, Université Paris–Diderot, 75005 Paris, France; and <sup>9</sup>Department of Applied Physics, Eindhoven University of Technology, 5600 MB Eindhoven, The Netherlands

Edited by Kari Dalnoki-Veress, McMaster University, Hamilton, ON, Canada, and accepted by Editorial Board Member John D. Weeks May 4, 2016 (received for review January 27, 2016)

**Solid particles floating at a liquid interface exhibit a long-ranged attraction mediated by surface tension. In the absence of bulk elasticity, this is the dominant lateral interaction of mechanical origin. Here, we show that an analogous long-range interaction occurs between adjacent droplets on solid substrates, which crucially relies on a combination of capillarity and bulk elasticity. We experimentally observe the interaction between droplets on soft gels and provide a theoretical framework that quantitatively predicts the interaction force between the droplets. Remarkably, we find that, although on thick substrates the interaction is purely attractive and leads to drop–drop coalescence, for relatively thin substrates a short-range repulsion occurs, which prevents the two drops from coming into direct contact. This versatile interaction is the liquid-on-solid analog of the “Cheerios effect.” The effect will strongly influence the condensation and coarsening of drops on soft polymer films, and has potential implications for colloidal assembly and mechanobiology.**

elastocapillarity | wetting | soft matter | mechanosensing | droplets

The long-ranged interaction between particles trapped at a fluid interface is exploited for the fabrication of microstructured materials via self-assembly and self-patterning (1–5) and occurs widely in the natural environment when living organisms or fine particles float on the surface of water (6, 7). In a certain class of capillary interactions, the particles deform the interface because of their shape or chemical heterogeneity (8–10). In this case, the change in interfacial area upon particle–particle approach causes an attractive capillary interaction between the particles. In the so-called Cheerios effect, the interaction between floating objects is mainly due to the change in gravitational potential energy associated to the weight of the particles, which deform the interface while being supported by surface tension (11), and the same principle applies when the interface is elastic (12–14). The name “Cheerios effect” is reminiscent of breakfast cereals floating on milk and sticking to each other or to the walls of the breakfast bowl.

Here, we consider a situation opposite to that of the Cheerios effect, liquid drops deposited on a solid. The solid is sufficiently soft to be deformed by the surface tension of the drops, resulting in a lateral interaction. Recent studies have provided a detailed view of statics of single-drop wetting on deformable surfaces (15–19). The length scale over which the substrate is deformed is set by the ratio of the droplet surface tension  $\gamma$  and the substrate shear modulus  $G$ . The deformation can be seen as an elastocapillary meniscus, or “wetting ridge,” around the drop (Fig. 1 *A* and *B*). Interestingly, the contact angles at the edge of the drop are governed by Neumann’s law, just as for oil drops floating on water. In contrast to the statics of soft wetting, its dynamics has only been explored recently. New effects such as stick–slip motion induced by substrate viscoelasticity (20, 21) and droplet migration due to stiffness gradients (22) have been revealed. The

possibility that elastocapillarity induces an interaction between neighboring drops is of major importance for applications such as drop condensation on polymer films (23) and self-cleaning surfaces (24–27). The interaction between drops on soft surfaces might also provide insights into the mechanics of cell locomotion (28–30) and cell–cell interaction (31).

Here, we show experimentally that long-ranged elastic deformations lead to an interaction between neighboring liquid drops on a layer of cross-linked polydimethylsiloxane (PDMS). The layer is sufficiently soft for significant surface tension-induced deformations to occur (Fig. 1). The interaction we observe can be thought of as the inverse Cheerios effect, because the roles of the solid and liquid phases are exchanged. Remarkably, the interaction can be either attractive or repulsive, depending on the geometry of the gel. We propose a theoretical derivation of the interaction force from a free-energy calculation that self-consistently accounts for the deformability of both the liquid drop and the elastic solid.

## Experiment: Attraction Versus Repulsion

Here, the inverted Cheerios effect is observed with submillimeter drops of ethylene glycol on a PDMS gel. The gel is a reticulated polymer network formed by crosslinking small multifunctional prepolymers—contrary to hydrogels, there is no liquid phase trapped inside the network. The low shear modulus of the PDMS

### Significance

The Cheerios effect is the attraction of solid particles floating on liquids, mediated by surface tension forces. We demonstrate experimentally that a similar interaction can also occur for the inverse case, liquid particles on the surface of solids, provided that the solid is sufficiently soft. Remarkably, depending on the thickness of the solid layer, the interaction can be either purely attractive or become repulsive. A theoretical model, in excellent agreement with the experimental data, shows that the interaction requires both elasticity and capillarity. Interactions between objects on soft substrates could play an important role in phenomena of cell–cell interaction and cell adhesion to biological tissues, and be exploited to engineer soft smart surfaces for controlled drop coalescence and colloidal assembly.

Author contributions: S.K., L.B., B.A., and J.H.S. designed research; S.K., A.P., L.A.L., J.H.W., L.B., S.D., and J.H.S. performed research; S.K. and A.P. analyzed data; and S.K., A.P., L.B., B.A., and J.H.S. wrote the paper.

The authors declare no conflict of interest.

This article is a PNAS Direct Submission. K.D.-V. is a guest editor invited by the Editorial Board.

Freely available online through the PNAS open access option.

<sup>1</sup>To whom correspondence should be addressed. Email: s.a.karpitschka@utwente.nl.

This article contains supporting information online at [www.pnas.org/lookup/suppl/doi:10.1073/pnas.1601411113/-DCSupplemental](http://www.pnas.org/lookup/suppl/doi:10.1073/pnas.1601411113/-DCSupplemental).

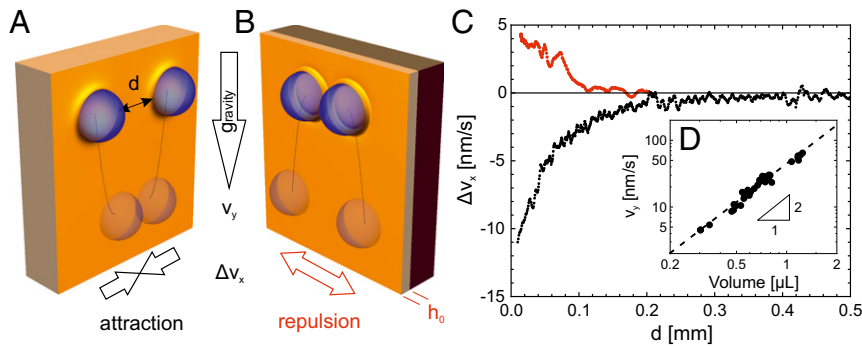


**Fig. 1.** The inverse Cheerios effect for droplets on soft solids. Two liquid drops sliding down a soft gel exhibit a mutual interaction mediated by the elastic deformation of the substrate. (A) Drops sliding down a thick elastic layer attract each other, providing a new mechanism for coalescence. (B) Drops sliding down a thin elastic layer (thickness  $h_0$ ) repel each other. (C) Measurement of the horizontal relative velocities  $\Delta v_x$  of droplet pairs, as a function of separation distance  $d$ . This measurement quantifies the interaction strength. (D) Sliding velocity of isolated droplets on the thick layer as a function of their volume. These data are used to calibrate the relation between force (gravity) and sliding velocity.

gel gives an elastocapillary length  $\ell = \gamma/G = 0.17$  mm sufficiently large to be measurable in the optical domain.

The interaction between two neighboring liquid drops is quantified by tracking their positions while they are sliding under the effect of gravity along the surface of a soft solid held vertically. The interaction can be either attractive (Fig. 1A) or repulsive (Fig. 1B): drops on relatively thick gel layers attract each other, whereas drops on relatively thin layers experience a repulsion.

The drop–drop interaction induces a lateral motion that can be quantified by measuring the horizontal component of the relative droplet velocity,  $\Delta v_x$  ( $\Delta v_x > 0$  implies repulsion). In Fig. 1C, we report  $\Delta v_x$  as a function of the separation  $d$ , defined as the shortest distance between the surfaces of the drops. The drops ( $R \approx 0.5 - 0.8$  mm) exhibit attraction when sliding down a thick layer ( $h_0 = 8$  mm, black curve), whereas they repel on a thin layer ( $h_0 = 0.04$  mm, red curve). The value of  $\Delta v_x$  is larger at close proximity, signaling an increase in the interaction force. Spontaneous merging occurs where drops come into direct contact. Importantly, these interactions provide a new mechanism for droplet coarsening (or ordering) by coalescence (or its suppression) that has no counterpart on rigid surfaces.

The interaction force  $F$  can be inferred from the relative velocities between the drops, by using an effective “drag law”, where the drag is due to sliding on the gel. We first calibrate this drag law by considering drops that are sufficiently separated, so that they do not experience any mutual interaction. The motion is purely downward and driven only by a gravitational force  $F_g = Mg$  (inertia is negligible). Fig. 1D shows that the droplet velocity  $v_y$  approximately scales as  $F_g^2$ . This force–velocity calibration curve is in good agreement with viscoelastic dissipation in the gel, based on which one expects the scaling law (21):

$$v \sim \frac{\ell}{\tau} \left( \frac{F}{2\pi R\gamma} \right)^{1/n}. \quad [1]$$

Here,  $n$  is the rheological exponent that emerges from the scale invariance of the gel network (32–34), and  $\tau$  is a characteristic timescale. The parameter values  $n \approx 0.61$  and  $\tau \approx 0.68$  s are calibrated in a rheometer (SI Materials and Methods). Eq. 1 is valid for  $v$  below the characteristic rheological speed,  $\ell/\tau$ . Our approach is justified here because  $\ell/\tau \sim 0.25$  mm/s for the silicone gel, whereas the reported speeds reach at most  $\sim 100$  nm/s. The large viscoelastic dissipation in the gel exceeds the dissipation within the drop by orders of magnitude, and explains these extremely slow drop velocities observed experimentally (21, 35). In this case, it was also shown that all of the dissipation occurs in a

very narrow region around the wetting ridge (21). Therefore, the dynamic substrate deformation approaches the corresponding static deformation beyond a distance  $v\tau \lesssim 60$  nm from the contact line. The force–distance relation for the inverse Cheerios effect can now be measured directly using the independently calibrated force–velocity relation (Fig. 1D and Eq. 1). By monitoring how the trajectories are deflected with respect to the downward motion of the drops, we obtain  $F$  (see Materials and Methods for additional details). Despite the different origins of calibration and interaction forces, both are balanced by the same dissipative mechanism because the dissipative viscoelastic force is nearly perfectly localized at the contact line (21), which corroborates the validity of our calibration routine.

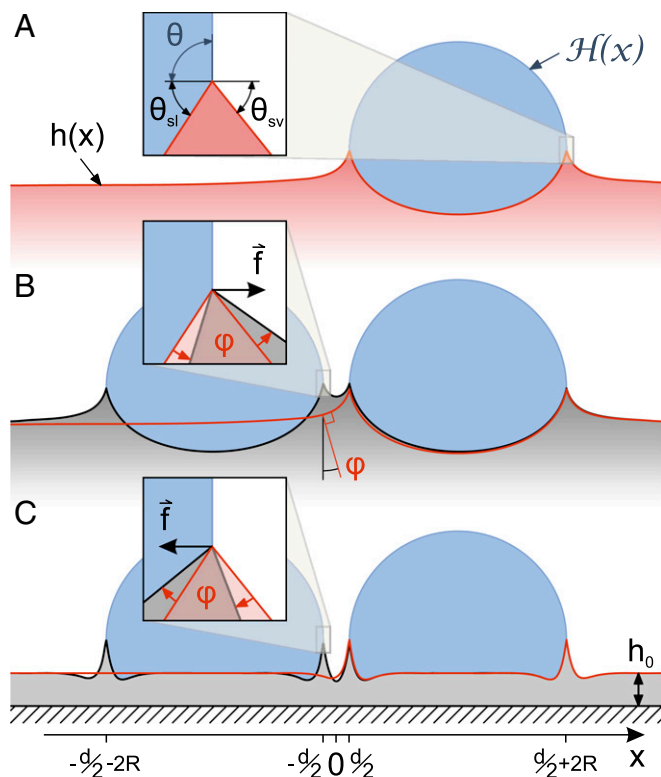
The key result is shown in Fig. 2, where we report the interaction force  $F$  as a function of distance  $d$ . Fig. 2A shows experimental data for the attractive force ( $F < 0$ ) between drops on thick layers (black dots), together with the theoretical prediction outlined below. Movie S1 shows an example of attractive drop–drop interaction. The attractive force is of the order of microneutons, which is comparable to both the capillary force scale  $\gamma R$  and the elastic force scale  $GR^2$ . The force decreases for larger distance and its measurable influence was up to  $d \sim R$ .

Fig. 2B shows the interaction force between drops on thin layers. The dominant interaction is now repulsive ( $d \gtrsim h_0$ ) (Movie S2). Intriguingly, we find that the interaction is not purely repulsive, but displays an attractive range at very small distance. It is possible to access this range experimentally in case the motion of the individual drops are sufficiently closely aligned (Movie S3). The “neutral” distance for which the interaction force changes sign appears when the separation is comparable to the substrate thickness  $h_0$ , suggesting that the key parameter governing whether the drops attract or repel is the thickness of the gel.

### Mechanism of Interaction: Rotation of Elastic Meniscus

We explain the attraction versus repulsion of neighboring drops by computing the total free energy  $\mathcal{E}$  of drops on gel layers of different thicknesses. The interaction force between the drops is equal to the energy gradient with respect to the separation,  $-\partial\mathcal{E}/\partial d$ , which in the experiment is balanced by the forces due to viscoelastic dissipation in the vicinity of the contact line. In contrast to the normal Cheerios effect, which involves two rigid particles, both the droplet and the elastic substrate are deformable, and their shapes will change upon varying the distance  $d$ . Hence, the interaction force involves both the elastic and the surface tension contributions to the free energy. The free energy emerges from self-consistently computed shapes of the drops and elastic deformations.





**Fig. 3.** Mechanism of interaction between two liquid drops on a soft solid. (A) Deformation  $h(x)$  induced by a single droplet on a thick substrate. The zoom near the contact line illustrates that the contact angles satisfy the Neumann condition. (B) A second drop placed on a thick substrate experiences a background profile due to the deformation induced by the neighboring drop on the right. This background profile is shown in red. As a consequence, the solid angles near the elastic meniscus rotate by an angle  $\phi$  (see zoom). This rotation perturbs the Neumann balance, yielding an attractive force  $\vec{f}$ . In the experiment, this force is balanced by the dissipative force due to the viscoelastic deformation of the wetting ridge. (C) On a thin substrate the single-drop profile yields a nonmonotonic elastic deformation. The zoom illustrates a rotation  $\phi$  of the Neumann triangle in the opposite direction, leading to a repulsive interaction.

discussed for rigid cylinders that deform an elastic surface due to gravity (14). In contrast, the inverted Cheerios effect discussed here does not involve gravity and can be totally ascribed to elastocapillary tilting of the solid interfaces, as shown in Fig. 3.

The rotation of contact angles explains why the drop–drop interaction can be either attractive or repulsive. On a thick substrate, the second drop experiences solid contact angles that are rotated counterclockwise, inducing an attractive force (Fig. 3B). In contrast, on a thin substrate, the elastic deformation induced by the second drop has a nonmonotonic profile  $h(x)$ . This is due to volume conservation of the substrate: lifting the gel near the contact line creates a depression at larger distances (Fig. 3C). The rotation of the contact angles thus changes sign, and, accordingly, the interaction force changes from attractive to repulsive. The relevant length scale for this phenomenon is set by the layer thickness  $h_0$ .

### Three-Dimensional Theory

The extension of the theory to three dimensions is straightforward and allows for a quantitative comparison with the experiments. For the 3D case, we compute the shape of the solid numerically, by first solving for the deformation field induced by a single drop using an axisymmetric elastic Green's function (18). Adding a second drop on this deformed surface gives an intricate deformation that is shown in Fig. 4 and Fig. S3. The imbalance of the Neumann law

applies everywhere around the contact line: the background deformation induces a rotation of the solid contact angles around the drop. According to Eq. 3, these rotations result into a distribution of force per unit length contact line  $\vec{f} = f(\beta)\vec{e}_r$ , where  $\vec{e}_r$  is the radial unit vector and  $\beta$  is the azimuthal angle (Fig. 4). The resultant interaction force  $\vec{F}$  is obtained by integration along the contact line,  $\vec{F} = R \int d\beta \vec{f}(\beta)$  (see Supporting Information and Fig. S4 for details). By symmetry, this force is oriented along the line connecting the two drops.

The interaction force obtained by the 3D theory is indicated by the red curves in Fig. 2A and B. The theory gives an excellent description of the experimental data without adjustable parameters. The quantitative agreement indicates that the interaction mechanism is indeed caused by the rotation of the elastic meniscus.

### Discussion

In summary, we have shown that liquid drops can exhibit a mutual interaction when deposited on soft surfaces. The interaction is mediated by substrate deformations, and its direction (repulsive versus attractive) can be tuned by varying the thickness of the layer. The measured force/distance relation is in quantitative agreement with the proposed elastocapillary theory. The current study reveals that multiple “pinchings” of an elastic layer by localized tractions  $\gamma$  lead to an interaction having a range comparable to  $\gamma/G$ . The key insight is that interaction emerges from the rotation of the elastic surface, providing a generic mechanism that should be applicable to a wide range of objects interacting on soft media.

Our model provides general concepts that are applicable to a wide range of experimental settings, whenever objects exert dipolar or quadrupolar forces on their substrate [the integral force must vanish in this case, however, as is the case, e.g., for cells (37)]. The length scale of interaction is governed by the ratio of two quantities: the force (per unit length)  $\gamma$ , and the substrate shear modulus  $G$ . This can range from nanometers for small forces or stiff substrates, to hundreds of microns for strong forces or soft substrates. In biological settings, elastocapillary interactions may play a role in cell–cell interactions, which are known to be sensitive to substrate stiffness (31). One example would be stem cell aggregates that interact with their extracellular matrix (38). In addition, the elastic interaction could also play a role in cell–extracellular matrix interactions, as a purely passive force promoting aggregation between anchor points on the surface of adhered biological cells. For example, it has been demonstrated that a characteristic distance of about 70 nm between topographical features enables the clustering of integrins. These transmembrane proteins are responsible for cell adhesion to the surrounding matrix, mediating the formation of

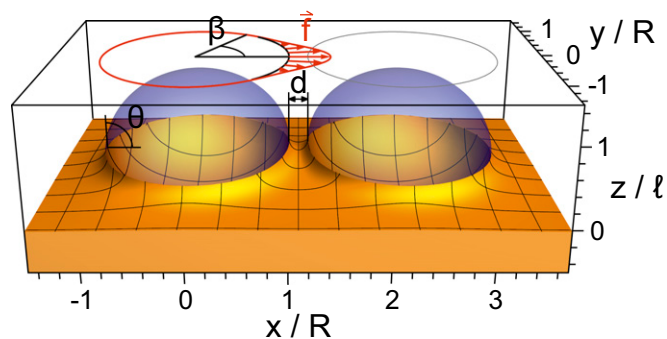


**Fig. 4.** Three-dimensional calculation of interface deformation for a pair of axisymmetric drops. The elastocapillary meniscus between the two drops is clearly visible, giving a rotation of the contact angle around the drop. The total interaction force  $\vec{F}$  is obtained by integration of the horizontal force  $\vec{f}$  (indicated in red) and is related to the free-energy gradient associated with a change in separation between the drops. Parameter values are  $l/R = 0.1$ ,  $\gamma/\gamma_s = 1$ .

strong anchor points when cells adhere to substrates (39, 40). Assuming that the topographical features “pinch” the cell with a force likely comparable to the cell’s cortical tension, which takes values in the range 0.1–1 mN/m (41–44), and an elastic modulus of  $10^3$ – $10^4$  Pa in the physiological range of biological tissues (45), one predicts a range of interaction consistent with observations.

More generally, substrate-mediated interactions could be dynamically programmed using the responsiveness of many gels to external stimuli (pH, temperature, electric fields). Possible applications range from fog harvesting and cooling to self-cleaning or anti-fouling surfaces, which rely on controlling drop migration and coalescence. The physical mechanisms revealed here, in combination with the fully quantitative elastocapillary theory we propose, pave the way for new design strategies for smart soft surfaces.

## Materials and Methods

**Supporting Information** provides further technical information, the derivation underlying Eq. 3, and the numerical scheme used for the calculations of Figs. 2 and 4. **Movies S1–S3** show typical experiments of drop–drop interactions.

**Substrate Preparation.** The two prepolymer components (Dow Corning; CY52-276 A and B) were mixed in a ratio of 1.3:1 (A:B). Thick elastic layers (~8 mm) were prepared in Petri dishes (diameter, ~90 mm). Thin layers (~40  $\mu$ m) were prepared by spin-coating the gel onto silicon wafers. The thickness was determined by color interferometry. See **SI Materials and Methods** for details on substrate curing and rheology (Fig. S5).

**Determining the Interaction Between Drops.** Droplets of ethylene glycol ( $V \sim 0.3$ – $0.8 \mu$ L) were pipetted onto a small region near the center of the cured substrate.

1. Tessier PM, et al. (2001) Structured metallic films for optical and spectroscopic applications via colloidal crystal templating. *Adv Mater* 13(6):396–400.
2. Furst EM (2011) Directing colloidal assembly at fluid interfaces. *Proc Natl Acad Sci USA* 108(52):20853–20854.
3. Cavallaro M, Jr, et al. (2013) Exploiting imperfections in the bulk to direct assembly of surface colloids. *Proc Natl Acad Sci USA* 110(47):18804–18808.
4. Bowden N, Terfort A, Carbeck J, Whitesides GM (1997) Self-assembly of mesoscale objects into ordered two-dimensional arrays. *Science* 276(5310):233–235.
5. Ershov D, Sprakel J, Appel J, Cohen Stuart MA, van der Gucht J (2013) Capillarity-induced ordering of spherical colloids on an interface with anisotropic curvature. *Proc Natl Acad Sci USA* 110(23):9220–9224.
6. Loudet JC, Pouligny B (2011) How do mosquito eggs self-assemble on the water surface? *Eur Phys J E Soft Matter* 34(8):76.
7. Peruzzo P, Defina A, Nepf HM, Stocker R (2013) Capillary interception of floating particles by surface-piercing vegetation. *Phys Rev Lett* 111(16):164501.
8. Danov KD, Kralchevsky PA, Naydenov BN, Brenn G (2005) Interactions between particles with an undulated contact line at a fluid interface: Capillary multipoles of arbitrary order. *J Colloid Interface Sci* 287(1):121–134.
9. Botto L, Lewandowski EP, Cavallaro M, Stebe KJ (2012) Capillary interactions between anisotropic particles. *Soft Matter* 8(39):9957–9971.
10. Kumar A, Park BJ, Tu F, Lee D (2013) Amphiphilic Janus particles at fluid interfaces. *Soft Matter* 9(29):6604–6617.
11. Vella D, Mahadevan L (2005) The Cheerios effect. *Am J Phys* 73(9):817–825.
12. Chakrabarti A, Chaudhury MK (2013) Surface folding-induced attraction and motion of particles in a soft elastic gel: Cooperative effects of surface tension, elasticity, and gravity. *Langmuir* 29(50):15543–15550.
13. Chakrabarti A, Chaudhury MK (2014) Elastocapillary interaction of particles on the surfaces of ultrasoft gels: A novel route to study self-assembly and soft lubrication. *Langmuir* 30(16):4684–4693.
14. Chakrabarti A, Ryan L, Chaudhury M, Mahadevan L (2015) Elastic cheerios effect: Self-assembly of cylinders on a soft solid. *Europhys Lett* 112(5):54001.
15. Jerison ER, Xu Y, Wilen LA, Dufresne ER (2011) Deformation of an elastic substrate by a three-phase contact line. *Phys Rev Lett* 106(18):186103.
16. Limat L (2012) Straight contact lines on a soft, incompressible solid. *Eur Phys J E Soft Matter* 35(12):9811.
17. Marchand A, Das S, Snoeijer JH, Andreotti B (2012) Contact angles on a soft solid: From Young’s law to Neumann’s law. *Phys Rev Lett* 109(23):236101.
18. Style RW, Dufresne ER (2012) Static wetting on deformable substrates, from liquids to soft solids. *Soft Matter* 8(27):7177–7184.
19. Lubbers LA, et al. (2014) Drops on soft solids: Free energy and double transition of contact angles. *J Fluid Mech* 747:R1.
20. Kajiya T, et al. (2014) A liquid contact line receding on a soft gel surface: Dip-coating geometry investigation. *Soft Matter* 10(44):8888–8895.
21. Karpitschka S, et al. (2015) Droplets move over viscoelastic substrates by surfing a ridge. *Nat Commun* 6:7891.
22. Style RW, et al. (2013) Patterning droplets with durotaxis. *Proc Natl Acad Sci USA* 110(31):12541–12544.

The sample was then mounted vertically so that gravity acts along the surface ( $-y$  direction; compare Fig. 1 A and B). The droplets were observed in transmission (thick layers) or reflection (thin layers) with collimated illumination, using a telecentric lens (JenMetar 1 $\times$ ) and a digital camera (pco 1200). Images were taken every 10 s. The contours of the droplets were determined by a standard correlation technique.

At large separation, droplets move downward due to gravity. The gravitational force on each droplet is proportional to its volume. The relation between force and velocity follows the same power law as the rheology, as was explained recently (21).

Individual droplets have different volumes and move with different velocities. Thus their distances change with time. Whenever two droplets approach each other, their trajectories change due to their interaction. Drops on thick substrates (Fig. 1C, black) attract and eventually merge. On a rigid surface, these droplets would not have merged. The opposite holds for droplets on thin layers (red): the droplets repel each other, which prevents coalescence.

To determine the interaction forces, we first evaluate the velocity vector of each individual droplet. The droplets move in a quasi-stationary manner, and the total force vector acting on each droplet is aligned with its velocity vector. The magnitude of the total force is obtained through calibration from the data shown in Fig. 1D. The interaction force is obtained by subtracting the gravitational force from the total force. Fig. 2A shows data from nine individual droplet pairs, corresponding to different times and different locations on the substrate. Fig. 2B shows data from 18 different droplet pairs. The raw data have been averaged over distance bins, taking the SD as error bar.

**ACKNOWLEDGMENTS.** L.B. acknowledges useful discussion on mechanobiology with Dr. Nuria Gavara, and financial support from European Union Grant CIG 618335. S.K. acknowledges financial support from NWO through VIDI Grant 11304. A.P. and J.H.S. acknowledge financial support from European Research Council Consolidator Grant 616918.

23. Sokuler M, et al. (2010) The softer the better: Fast condensation on soft surfaces. *Langmuir* 26(3):1544–1547.
24. Schellenberger F, et al. (2015) Direct observation of drops on slippery lubricant-infused surfaces. *Soft Matter* 11(38):7617–7626.
25. Rykaczewski K, et al. (2014) Dropwise condensation of low surface tension fluids on omniphobic surfaces. *Sci Rep* 4:4158.
26. Kim P, et al. (2012) Liquid-infused nanostructured surfaces with extreme anti-ice and anti-frost performance. *ACS Nano* 6(8):6569–6577.
27. Subramanyam SB, Rykaczewski K, Varanasi KK (2013) Ice adhesion on lubricant-impregnated textured surfaces. *Langmuir* 29(44):13414–13418.
28. Discher DE, Janmey P, Wang YL (2005) Tissue cells feel and respond to the stiffness of their substrate. *Science* 310(5751):1139–1143.
29. Lo CM, Wang HB, Dembo M, Wang YL (2000) Cell movement is guided by the rigidity of the substrate. *Biophys J* 79(1):144–152.
30. Zhang R, Ni L, Jin Z, Li J, Jin F (2014) Bacteria slingshot more on soft surfaces. *Nat Commun* 5:5541.
31. Guo WH, Frey MT, Burnham NA, Wang YL (2006) Substrate rigidity regulates the formation and maintenance of tissues. *Biophys J* 90(6):2213–2220.
32. Winter H, Chambon F (1986) Analysis of linear viscoelasticity of a cross-linking polymer at the gel point. *J Rheol (NYY)* 30(2):367–382.
33. Long D, Ajdari A, Leibler L (1996) Static and dynamic wetting properties of thin rubber films. *Langmuir* 12(21):5221–5230.
34. de Gennes PG (1996) Soft adhesives. *Langmuir* 12(19):4497–4500.
35. Carre A, Gastel J, Shanahan M (1996) Viscoelastic effects in the spreading of liquids. *Nature* 379(6564):432–434.
36. Andreotti B, Snoeijer JH (2016) Soft wetting and the Shuttleworth effect, at the crossroads between thermodynamics and mechanics. *Europhys Lett* 113(6):66001.
37. Henry S, Chen C, Crocker J, Hammer D (2015) Dynamic traction forces of human neutrophil adhesion. *Biophys J* 108(2):495a.
38. Przybyla L, Lakin JN, Sunyer R, Trepas X, Weaver VM (2016) Monitoring developmental force distributions in reconstituted embryonic epithelia. *Methods* 94:101–113.
39. Huang J, et al. (2009) Impact of order and disorder in RGD nanopatterns on cell adhesion. *Nano Lett* 9(3):1111–1116.
40. Dalby MJ, Gadegaard N, Oreffo RO (2014) Harnessing nanotopography and integrin-matrix interactions to influence stem cell fate. *Nat Mater* 13(6):558–569.
41. Krieg M, et al. (2008) Tensile forces govern germ-layer organization in zebrafish. *Nat Cell Biol* 10(4):429–436.
42. Tinevez JY, et al. (2009) Role of cortical tension in bleb growth. *Proc Natl Acad Sci USA* 106(44):18581–18586.
43. Fischer-Friedrich E, Hyman AA, Jülicher F, Müller DJ, Helenius J (2014) Quantification of surface tension and internal pressure generated by single mitotic cells. *Sci Rep* 4:6213.
44. Sliogeryte K, Thorpe SD, Lee DA, Botto L, Knight MM (2014) Stem cell differentiation increases membrane-actin adhesion regulating cell blebability, migration and mechanics. *Sci Rep* 4:7307.
45. Swift J, et al. (2013) Nuclear lamin-A scales with tissue stiffness and enhances matrix-directed differentiation. *Science* 341(6149):1240104.
46. Sneddon IN (1951) *Fourier Transforms* (McGraw-Hill, New York).